

# Simulation of the Three-Dimensional Hinge Flow Fields of a Bileaflet Mechanical Heart Valve Under Aortic Conditions

HÉLÈNE A. SIMON,<sup>1</sup> LIANG GE,<sup>3</sup> FOTIS SOTIROPOULOS,<sup>4</sup> and AJIT P. YOGANATHAN<sup>1,2</sup>

<sup>1</sup>School of Chemical and Biomolecular Engineering, Georgia Institute of Technology, Atlanta, GA, USA; <sup>2</sup>The Wallace H. Coulter Department of Biomedical Engineering, Georgia Institute of Technology, Atlanta, GA, USA; <sup>3</sup>University of California San Francisco, San Francisco, CA, USA; and <sup>4</sup>St. Anthony Falls Laboratory, Department of Civil Engineering, University of Minnesota, Minneapolis, MN, USA

(Received 11 March 2009; accepted 23 November 2009; published online 4 December 2009)

**Abstract**—Thromboembolic complications of bileaflet mechanical heart valves (BMHV) are believed to be due to detrimental stresses imposed on blood elements by the hinge flows. Characterization of these flows is thus crucial to identify the underlying causes for complications. In this study, we conduct three-dimensional pulsatile flow simulations through the hinge of a BMHV under aortic conditions. Hinge and leaflet geometries are reconstructed from the Micro-Computed Tomography scans of a BMHV. Simulations are conducted using a Cartesian sharp-interface immersed-boundary methodology combined with a second-order accurate fractional-step method. Physiologic flow boundary conditions and leaflet motion are extracted from the Fluid-Structure Interaction simulations of the bulk of the flow through a BMHV. Calculations reveal the presence, throughout the cardiac cycle, of flow patterns known to be detrimental to blood elements. Flow fields are characterized by: (1) complex systolic flows, with rotating structures and slow reverse flow pattern, and (2) two strong diastolic leakage jets accompanied by fast reverse flow at the hinge bottom. Elevated shear stresses, up to 1920 dyn/cm<sup>2</sup> during systole and 6115 dyn/cm<sup>2</sup> during diastole, are reported. This study underscores the need to conduct three-dimensional simulations throughout the cardiac cycle to fully characterize the complexity and thromboembolic potential of the hinge flows.

**Keywords**—Pulsatile numerical simulations, Fluid mechanics, Pivot, Computational fluid dynamics CFD, Physiologic conditions.

## INTRODUCTION

Nearly 45% of all failing native heart valves are currently replaced by a bileaflet mechanical heart valve (BMHV). However, despite their widespread use,

BMHVs are not complication-free and are still associated with high levels of hemolysis, platelet activation and thromboembolic events. Clinical reports and recent *in vitro* experiments suggest that these complications are associated with the fluid stresses imposed on blood elements by the non-physiological hemodynamics induced by the valve, in particular its hinge region.

With that observation in mind, numerous researchers have sought to characterize the flow field inside the hinge region in an effort to better understand the relationship between hinge design and thromboembolic potential. However, because of the small dimensions of the hinge region, the opacity and the motion of the leaflets, experimental studies provided only limited information on the flow field. Most studies, for example, have only captured two-dimensional velocity fields at selected locations.<sup>5,8,15,21,27,30</sup> Researchers have therefore undertaken numerical studies to obtain further information on the hinge flow fields. However, the relevance of most of the numerical simulations to date is insufficient due to a lack of spatial resolution or the use of non-physiologic flow conditions. Wang *et al.* investigated the flow fields of a protruded hinge but limited their study to steady flow conditions with non-moving fully-open leaflets.<sup>33</sup> Kelly *et al.* simulated the flow in the recessed hinge region of a 25 mm ATS valve placed under aortic conditions,<sup>18</sup> but the authors only modeled the forward flow phase and assumed a simplified sinusoidal pulse wave. However, flow pulsatility and leaflet motion throughout the cardiac cycle are key factors influencing the hinge hemodynamics. The simplified boundary conditions of these first simulations constitute a major impediment to their relevance and application. Accordingly, a number of recent studies have sought to impose physiologic flow conditions and leaflet motion based on experimental data.<sup>9,15,29</sup> These studies

Address correspondence to Ajit P. Yoganathan, The Wallace H. Coulter Department of Biomedical Engineering, Georgia Institute of Technology, 313 Ferst Drive, BME Building, Room 2119, Atlanta, GA 30332-0535, USA. Electronic mail: ajit.yoganathan@bme.gatech.edu

showed the presence of highly three-dimensional flow structures throughout the cardiac cycle but lack high spatial resolution inside of the hinge recess. More importantly, none of these studies presented detailed maps of the shear stress levels computed in the near-hinge region. Such maps could help in pinpointing regions with elevated thrombogenic potential and be used to design hinges with lesser risk of blood damage.

As highlighted by the previously published studies and a recent review by Sotiropoulos and Borazjani,<sup>31</sup> simulating the flow through BMHVs is computationally challenging. These challenges stem principally from (1) the large disparity of scales, from several millimeters in the valve diameter down to a few hundred microns in the hinge recess, (2) the motion of the leaflet requiring sophisticated Fluid–Structure Interaction (FSI) modeling, and (3) the transition to turbulence in the bulk of the valvular flow. It is therefore extremely difficult, if not impossible with the currently available computational resources, to perform a full multi-scale simulation of the BMHV flow by simultaneously capturing the large-scale flow features in the bulk of the flow and the small-scale flow features occurring inside of the hinge recess while retaining good spatial and temporal resolutions.

In the present study, a pseudo-multiscale approach is thus implemented to simulate the three-dimensional pulsatile physiologic flow in the hinge region of a BMHV. This is achieved by performing a one-way coupling between large-scale and small-scale simulations consisting of extracting the boundary conditions for the hinge simulations from the FSI simulations of a BMHV bulk flow. We first present the numerical method to solve the governing equations, the boundary conditions and the hinge numerical model. We then describe in details the flow inside of the hinge region, highlighting characteristic three-dimensional flow features and emphasizing regions of high shear stress levels.

## METHODS

### *Flow Solver*

The numerical method is an extension of the methodology developed by Sotiropoulos and co-workers.<sup>3,11,12</sup> This method was recently applied to carry out the first, high-resolution FSI simulations of large-scale BMHV flows at physiologic conditions<sup>3</sup> and yielded results in excellent agreement with *in vitro* measurements.<sup>4</sup>

In this study, the fluid motion is described by the incompressible, Newtonian form of the time-dependent Navier–Stokes equations. These equations are

solved using a hybrid staggered/non-staggered control-volume method.<sup>11</sup> The convective terms are approximated using a second-order accurate upwind QUICK scheme, while three-point central second-order accurate differencing is used to discretize the divergence operator in the continuity equation, pressure gradient, and the viscous terms. The governing equations are integrated in time using an efficient, second-order accurate fractional step method. In this approach, the momentum equations, discretized using a second-order backward Euler scheme for the temporal term, are solved using the restarted Generalized Minimal Residual Method (GMRES) solver with a block Jacobi preconditioner. The pressure Poisson equation is solved using a GMRES solver enhanced with a multigrid approach as preconditioner. The flow solver is fully parallelized and the overall methodology for solving the momentum equations is implemented using the libraries available in PETSC (Portable, Extensible Toolkit for Scientific Computation).<sup>1,2</sup>

This flow solver is coupled with the hybrid Cartesian sharp-interface immersed-boundary approach proposed by Gilmanov and Sotiropoulos.<sup>12</sup> The walls of the immersed geometry (here, leaflet, valve housing, and valve chamber) are discretized with an unstructured, triangular mesh and treated as sharp interfaces immersed in the background grid domain. At every time step, all nodes of the Cartesian grid domain are sorted into three categories based on their location relative to the boundary: (1) nodes in the fluid (*fluid* nodes), (2) nodes in the solid body (*body* nodes), and (3) near-boundary nodes (*nb* nodes). Once all Cartesian nodes have been classified, the governing equations are solved at all *fluid* nodes with all *body* nodes excluded from the computational domain. The flow variables at the *nb* nodes are reconstructed via interpolation along the local normal direction to the body surface to appropriately represent the effect of the moving leaflet on the surrounding fluid.<sup>12</sup>

### *Hinge Geometry and Flow Domain (Fig. 1)*

The St. Jude Medical (SJM) valve was selected for this study as it is currently one of the most implanted BMHV. Micro-Computed Tomography technique was used to obtain a scan of the hinge region and leaflet ear of a SJM valve. RainDrop Geomagics (Geomagics Studio 10 SR2) was used to extract and smoothen the hinge recess and leaflet ear surfaces from the scan. The final unstructured triangular mesh was generated using Pro|Engineer (Pro|Engineer Wildfire 3.0 M020) and Gambit (Gambit 2.4.6, Fluent Inc) software. The leaflet ear was positioned within the hinge recess such that the hinge gap width (distance between the bottom of the hinge recess and the tip of the leaflet ear, defined

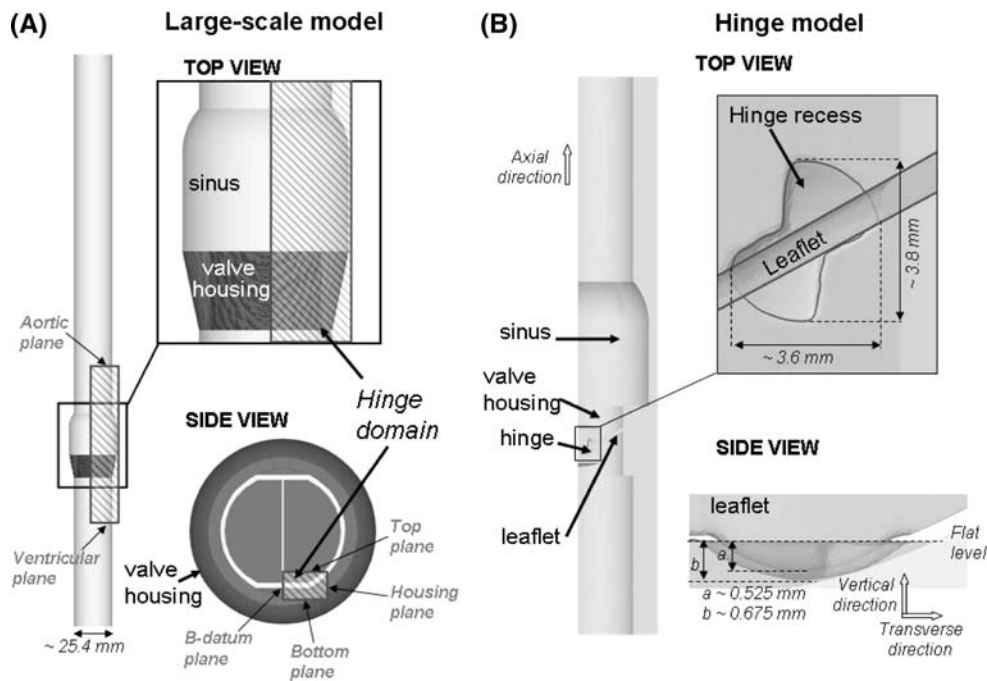


**FIGURE 1.** Large-scale (A) and present hinge (B) numerical models. (A) In the large-scale numerical model, a SJM valve model is inserted into a simplified aorta consisting of a straight tube with an axisymmetric expansion representing the sinus region. The model for the hinge simulations corresponds to the shaded area in the large-scale model. (B) The hinge model is shown and the hinge recess, characterized by its butterfly shape, is clearly visible.

as (b-a) in Fig. 1) was approximately that seen in clinical valves ( $150 \mu\text{m}$ ).

The numerical model was set to correspond to a section of a BMHV inserted into a simplified aorta model composed of a straight pipe with an axisymmetric expansion representing the sinus region. Only one of the four hinges was modeled. The geometry of the valve chamber, housing, and leaflet was immersed into a fluid domain composed of a non-uniform Cartesian grid of approximately 5.9 million grid nodes. The fluid grid was stretched to ensure that the grid within the hinge recess was sufficiently fine to resolve all fine details of the hinge structure. Approximately 80,000 grid nodes were located within the hinge recess itself, the resolution of the grid at the bottom of the hinge recess being approximately  $8 \mu\text{m}$ .

#### Boundary Conditions

The conditions applied at the fluid domain boundaries were obtained from the large-scale FSI simulations of the bulk of the flow through a BMHV subjected to aortic physiologic conditions.<sup>3</sup> In these large-scale simulations, the detailed geometry of the hinge recess was neglected as shown in Fig. 1 and the following normal aortic physiologic flow conditions were imposed: peak flow rate of approximately

25 L/min, systolic duration of one-third of the cardiac cycle, a cardiac cycle of 860 ms, and a heart rate of 70 beats/min. The velocity fields and leaflet position calculated with the large-scale FSI solver during systole<sup>1</sup> were found to be in excellent agreement with Particle Image Velocimetry experimental data published by Dasi *et al.*<sup>3,4</sup> During this phase, velocity profiles were therefore extracted from the large-scale simulation and used as boundary flow conditions for the ventricular plane of the hinge domain. This approach ensured a one-way coupling between the large-scale and the hinge models. On the other hand, prescribing the interpolated velocity during the leakage phase was not deemed suitable as the peripheral gap (the gap between the closed leaflets and the valve housing) in the large-scale model was larger than in actual clinical valves. Starting at the instance of time when the valvular flow rate is zero toward the end of systole, a plug flow profile was applied at the aortic plane of the hinge domain. The magnitude of this plug flow was linearly increased from 0 at the time of zero-flow-rate ( $t = 344 \text{ ms}$ ) to  $V_{\min}^P = -0.11 \text{ m/s}$  at the instance of valve closure ( $t = 384 \text{ ms}$ ), and kept constant after valve closure.  $V_{\min}^P$  was chosen so as to reach a physiologic pressure gradient of 80 mmHg across the closed valve at mid-diastole. Figure 2 displays the temporal variations of the cross-valvular flow rate and leaflet position imposed in the present study. Due to

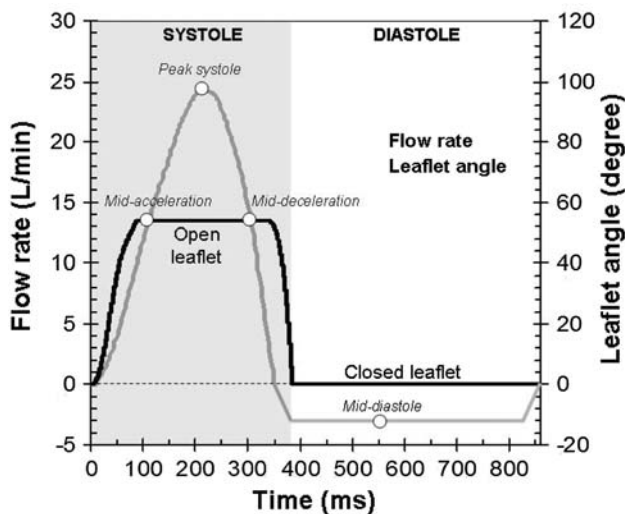


**FIGURE 2.** Valvular flow and pressure waveforms. The cardiac cycle duration was set to 860 ms, which corresponds to a heart rate of 70 beat/min. The instances of time corresponding to mid-acceleration, peak systole, mid-deceleration and mid-diastole are included.

computational limitations, only one cardiac cycle is here modeled.

Zero-transverse flux was enforced across the top and b-datum planes while zero-velocity conditions were applied at the bottom and housing planes. The flow velocity at the outlet plane (the downstream/upstream plane during systole/diastole, respectively) was scaled in order to ensure mass conservation throughout the domain. The leaflet position computed with the FSI solver was used to prescribe the leaflet motion during systole.<sup>3</sup> The leaflet was kept in a non-moving closed position after valve closure. The position of the leaflet as a function of time is given in Fig. 2. The leaflet is seen to span  $54.2^\circ$  from  $0^\circ$  in its fully-closed position to  $54.2^\circ$  in its fully-open position. It should be noted that the fully-open leaflet makes an angle of  $4.8^\circ$  with the main stream flow direction. The no-slip condition was enforced along all body surfaces.

## RESULTS

The nomenclature used to describe the hinge recess geometry and the flow patterns in the result section is provided in Figs. 1 and 3A. The plane of reference is chosen as the *flat level*, which is the level flushed with the valve housing. The direction perpendicular to the flat level and parallel to the leaflet axis is referred to as the *vertical direction*. The *axial direction* is the direction parallel to the main flow and the *transverse direction* corresponds to the direction from the b-datum plane to the valve housing.

### *Hinge Flow Fields During the Forward Flow Phase*

As expected, the flow structures observed in our simulations are highly three-dimensional with strong flow in the vertical direction. This is clearly visible in Fig. 3, which shows the global hinge flow structures at peak systole using three-dimensional instantaneous streamtraces. The streamtraces that enter the hinge from the ventricular side (colored in blue) collide with the upstream edge of the leaflet (label a), dive inside the hinge recess in the ventricular corner, traverse the hinge (label b), and finally exit through the adjacent corner (label c). The red streamtraces in the lateral corner of the hinge show that the flow swirls (label d), goes underneath of the leaflet ear (label e), and finally exits the hinge through the adjacent corner (label c). The three-dimensionality of the flow is clearly visible within the recess but also outside of the hinge as the streamtraces nearly parallel to the flat level (label f) in the ventricular side of the hinge change direction forming an angle as high as  $45^\circ$  with the flat level in the aortic side of the hinge (label g).

To gain better insights into the hinge flow fields, Fig. 4 shows two-dimensional in plane velocity vectors with out-of-plane velocity component contours at the flat level (Fig. 4A) and the out-of-plane vorticity contours (Fig. 4B). From this figure, a region of elevated velocity can be identified in the adjacent corner (label h). The downstream-most part of this corner is characterized by a rotating flow with large out-of-plane vertical velocity component (up to 0.71 m/s at the flat level at peak systole). Such a flow distribution in the adjacent corner is likely due to the impingement of the flow against the wall of the recess before exiting the hinge, as suggested by the blue streamtraces in Fig. 3A (label c). In the lateral corner of the hinge, a strong axial flow (label i) with smaller out-of-plane velocity component is seen ( $-0.16$  m/s at the flat level at peak systole).

Expectedly, the velocity magnitude through the hinge recess closely follows the magnitude of the valvular flow rate during the forward flow phase. The maximum velocity magnitudes within the hinge recess reach 0.75, 1.54, and 0.88 m/s at mid-acceleration, peak systole and mid-deceleration, respectively. This global increase in flow rate at mid-systole also translates into a higher three-dimensionality of the flow within the hinge recess. This is in particular evidenced by the increased out-of-plane velocity components: the maximum absolute vertical velocity component within the hinge recess is nearly twice as high at peak systole (0.71 m/s) compared to mid-acceleration (0.38 m/s) and mid-deceleration (0.34 m/s).

It is interesting to note that despite the significant forward flow pattern observed throughout the hinge

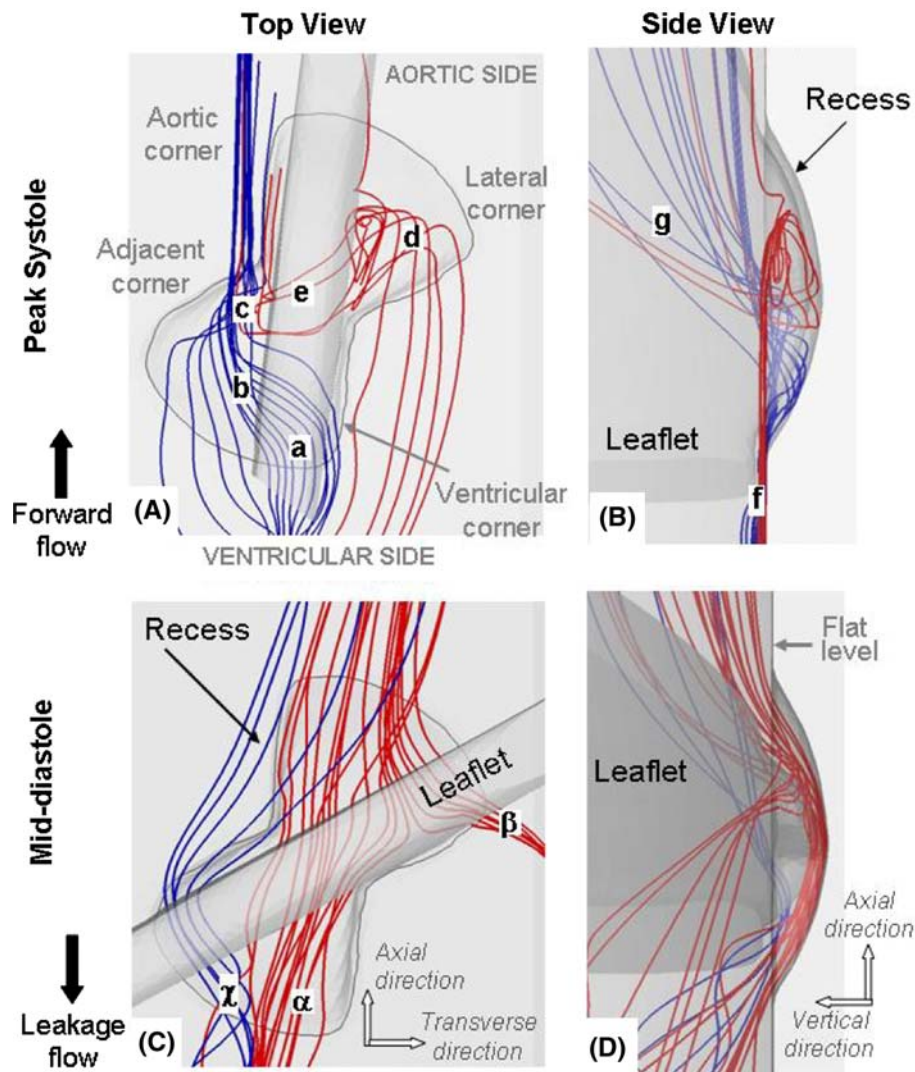


**FIGURE 3.** Three-dimensional streamtraces at peak systole (A and B) and mid-diastole (C and D). The streamtraces entering the ventricular side of the hinge are color-coded in blue while those entering the hinge through the aortic side are shown in red. The terminology used to describe the hinge recess is included in panel A.

during systole, a pocket of reverse flow of low magnitude is seen at the bottom of the recess through the gap formed by the leaflet ear surface and the recess wall (Figs. 4C and 4D). This reverse flow correlates with the direction of the red streamtraces shown in Fig. 3A (label e) and underscores the three-dimensionality and complexity of the hinge flow fields during the forward flow phase. The velocity magnitude in this region does not exceed 0.22 m/s at mid-acceleration and mid-deceleration, and 0.41 m/s at peak systole. The presence of this flow reversal is further confirmed in Fig. 5 where two-dimensional in-plane velocity vectors and out-of-plane velocity contours are plotted at four different planes within the hinge recess. Reverse velocity vectors are observed at the deepest level (label l) despite the large forward flow pattern displayed at the flat level (labels j and k).

#### *Hinge Flow Fields During the Leakage Flow Phase*

The diastolic phase is characterized by reverse leakage flows throughout the hinge. The streamtraces in Fig. 3 highlight the three-dimensionality of the hinge flow during the leakage flow phase. The red streamtraces clearly show the fluid diving into the recess from the aortic side of the hinge, flowing underneath the leaflet ear and exiting the recess through the ventricular (label  $\alpha$ ) and lateral (label  $\beta$ ) corners of the hinge. The blue streamtraces depict another leakage jet in the adjacent corner of the hinge (label  $\gamma$ ).

Focusing on the flat level (Fig. 5), the adjacent (label  $\phi$ ) and lateral (label  $\varepsilon$ ) leakage jets are clearly visible on either side of the closed leaflet, with a maximum velocity magnitude of 4.75 and 3.98 m/s,

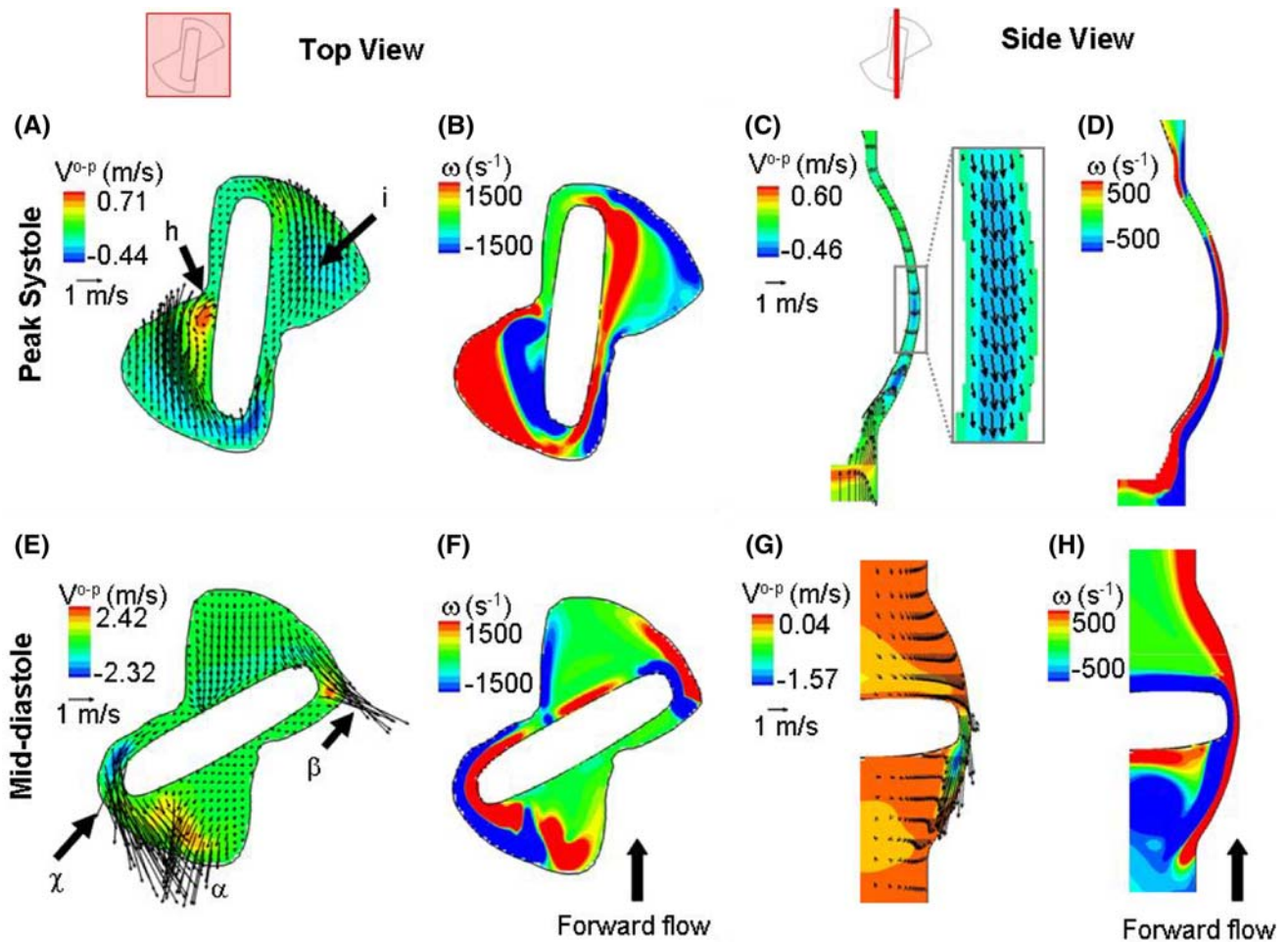


**FIGURE 4.** Hinge flow fields at peak systole and mid-diastole. As depicted on the two hinge diagrams, the top view shows the flow fields at the flat level while the side view shows the flow fields along a cross-sectional plane located in the center of the hinge. Two dimensional in-plane velocity vectors along with out-of-plane velocity component ( $V^{o-p}$ ) contours and out-of-plane vorticity ( $\omega$ ) contour plots are shown at peak systole (top row) and diastole (bottom row). The out-of-plane component corresponds to the vertical component in panels A, B, E and F and to the radial component in panels C, D, G and H.

respectively. These high speed leakage jets have large out-of-plane vertical component as shown by the out-of-plane velocity contours (Fig. 4E) which range from  $-2.32$  to  $2.42$  m/s. A third leakage jet of lesser magnitude (label  $\delta$  in Fig. 5) is visible in the ventricular corner of the hinge. This ventricular jet corresponds to the fluid entering the hinge through the aortic corner, flowing underneath the closed leaflet ear, and exiting the hinge recess through the ventricular corner. The flow leaking underneath of the closed leaflet is clearly visible in the side view shown in Figs. 4G and 4H.

The leakage flow pattern in the hinge recess is also visible in Fig. 5 (bottom row), where high reverse velocities are observed at all planes within the hinge recess, including the deepest plane. It is during the leakage phase that the flow is the most three-dimensional, as evidenced by the maximum absolute vertical velocity component being three-times larger during

diastole compared to systole (Fig. 4), with a maximum up to  $2.42$  m/s at the flat level at mid-diastole. The transverse velocity components along the hinge cross-sectional center plane are also larger during mid-diastole compared to peak systole, ranging from  $-1.57$  to  $0.04$  m/s.

#### Shear Stress Levels

Figures 6 and 7 present the principal shear stress contour maps and iso-surfaces at peak systole and mid-diastole. The principal shear stress levels are computed according to the method proposed by Higdon *et al.*<sup>16</sup> and are referred simply as shear stress levels in the remainder of the paper. Note that the maximum of the color-scale is set to  $1000$  dyn/cm<sup>2</sup> to highlight regions with elevated potential for platelet activation as previous researchers have shown that

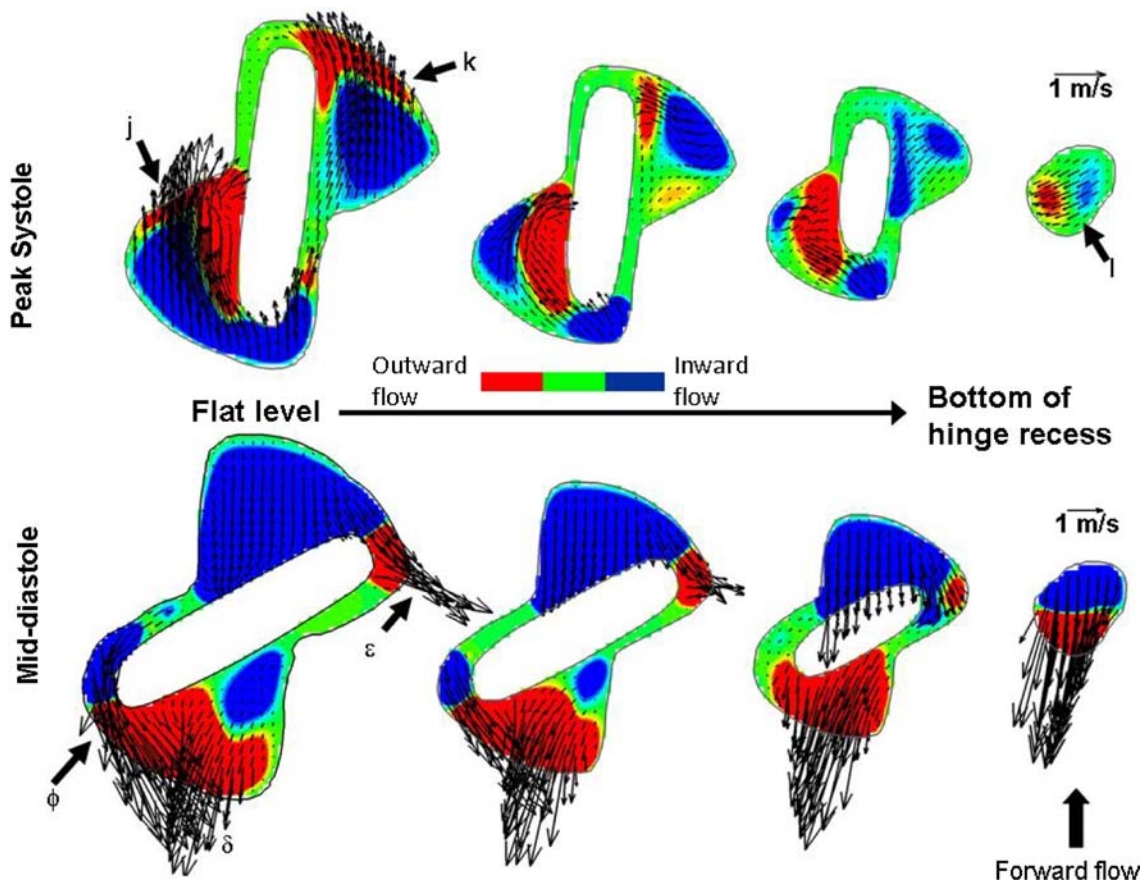


**FIGURE 5.** Hinge flow fields along four different planes within the hinge recess at peak systole and mid-diastole. The four planes depicted are: flat level, 195, 390, and 585  $\mu\text{m}$  within the hinge recess. Two-dimensional in-plane velocity vectors are presented. The contours are representative of the out-of-plane velocity component, blue indicating inward flow (going inside the hinge recess) and red outward flow (going out of the hinge recess).

shear stress as low as 100–1000  $\text{dyn}/\text{cm}^2$  depending upon the exposure time may induce platelet activation.<sup>17,26,34,35</sup>

The shear stress level distribution is similar throughout the forward flow phase, but it is at peak systole that the maxima occur. At this particular instance of the cardiac cycle, a region of high shear stresses (with a peak of 1920  $\text{dyn}/\text{cm}^2$ ) is present near the flat level, outside and immediately upstream of the recess. The region underneath of the open leaflet, upstream of the hinge, is also characterized by elevated shear stresses (up to 1170  $\text{dyn}/\text{cm}^2$ ). The hinge recess itself, on the other hand, is associated with lower shear stress values and its shear stress distribution is characterized by higher levels in the ventricular side compared to the aortic side. A local maximum of 775  $\text{dyn}/\text{cm}^2$  is recorded along the wall of the ventricular corner close to the flat level. The maximum shear stress within the hinge recess is located near the tip of the leaflet ear with a peak of 370  $\text{dyn}/\text{cm}^2$ .

It is during the leakage phase that the maximum shear stress levels are seen. During this phase, very

large shear stresses are observed where the flow squeezes between the closed leaflet and the valve housing and forms two strong leakage jets on either sides of the leaflet ear. The shear stress levels reach up to 5030  $\text{dyn}/\text{cm}^2$  in the lateral jet and 6115  $\text{dyn}/\text{cm}^2$  in the adjacent jet along the leaflet surface. Values up to 2930 and 2215  $\text{dyn}/\text{cm}^2$  are seen at the flat level along the adjacent and lateral recess walls, respectively. Elevated levels of shear stress are also present at the center of the hinge, in the gap formed between the bottom of the hinge recess and the leaflet ear surface. In this region, the maximum shear stress is seen near the tip of the leaflet ear with a peak of 4865  $\text{dyn}/\text{cm}^2$ .

## DISCUSSION

In this study three-dimensional, time-accurate simulations were carried out to model the flow through the hinge recess of a SJM valve under aortic physiologic flow conditions. These simulations underscore the three-dimensionality of the hinge flow fields and the

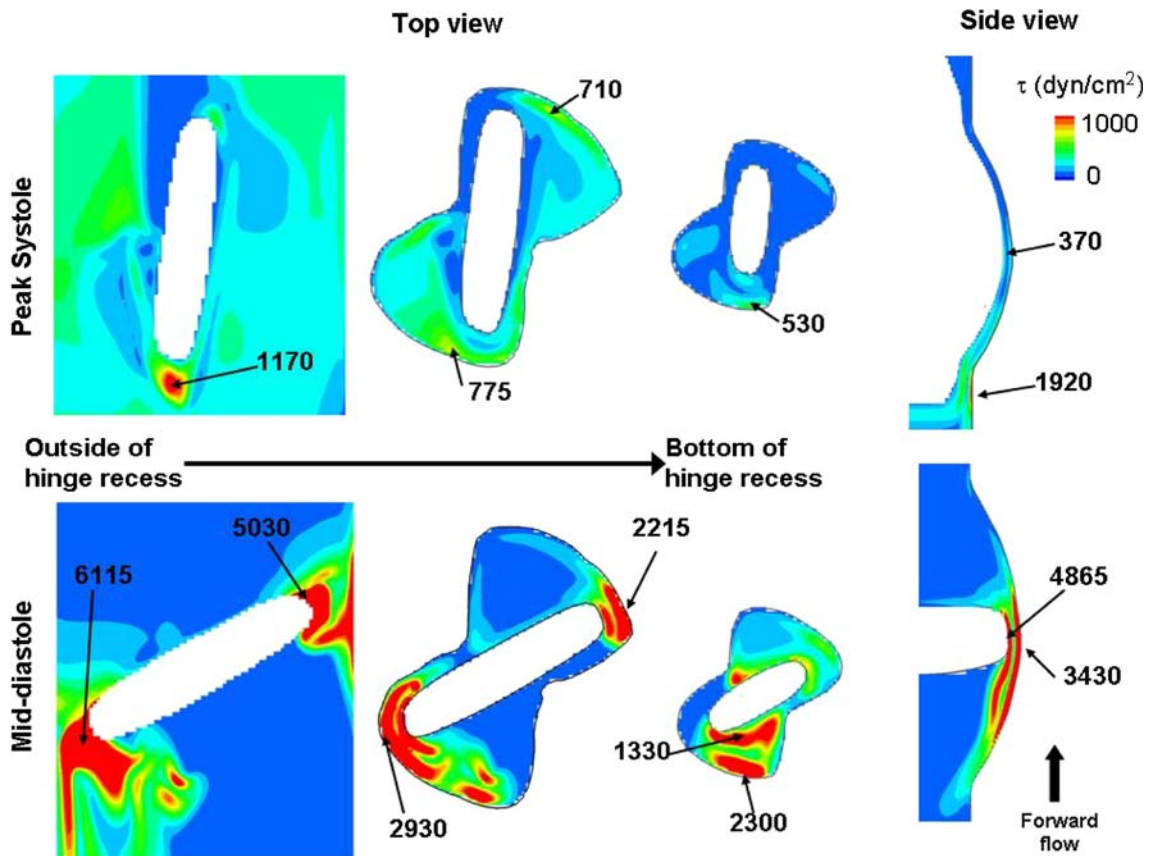


FIGURE 6. Shear stress distribution. Shear stress level contours are shown along three planes: (1) outside of the recess, near the leaflet edge surface, (2) at the flat level, and (3) at  $390\ \mu\text{m}$  within the hinge recess. Also included is a cross-sectional view through the center plane of the hinge. The local maxima, with their approximate location, are given.

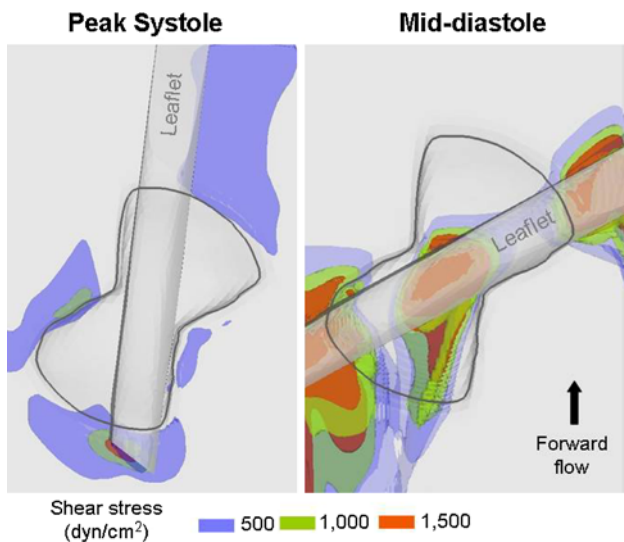


FIGURE 7. Iso-surfaces of shear stress levels at peak systole and mid-diastole. Iso-surfaces of three shear stress levels (blue,  $500\ \text{dyn/cm}^2$ ; green,  $1,000\ \text{dyn/cm}^2$ ; red,  $1,500\ \text{dyn/cm}^2$ ) are displayed in the near-hinge region at peak systole and mid-diastole.

intense unsteadiness observed throughout the cardiac cycle. The simulations highlight the need for carrying out highly resolved three-dimensional simulations modeling the entire cardiac cycle. Simulations limited to steady flow conditions<sup>33</sup> or to a section of the cardiac cycle, such as the forward flow phase,<sup>18</sup> cannot accurately capture the flow unsteadiness that are characteristic of the hinge flow fields. Imposing physiologic flow conditions should therefore be attempted whenever possible.

Modeling physiologic boundary conditions is of prime importance to assess the *in vivo* performance of a specific hinge design. By performing a one-way coupling between a large-scale model and the hinge solver and using knowledge of the human physiology, the present study reproduces the hemodynamic environment of the hinge as closely as possible. During systole, the hinge has little effect on the bulk flow through the open valve, so that a one-way coupling between the large-scale and the hinge flow solver was deemed appropriate. However, such an approach is not applicable during diastole. The exact leakage flow rate

through the closed valve is dependent on the cross-valvular pressure gradient and the resistance offered to the flow by the hinge, the b-datum gap, and the peripheral gap. This in turn is dependent on the geometry and dimensions of these gaps. Simulating the flow in gaps similar in size to those present in a clinical quality valve, while achieving good spatial resolution, would exceed currently available computational resources. The gap dimensions in the large-scale model therefore had to be increased and physiological cross-valvular pressure gradient could not be achieved. As a result, prescribing the large-scale velocity profile as boundary conditions for the present hinge model during the leakage phase was not deemed suitable and, instead, the boundary conditions were set such as to impose a cross-valvular pressure gradient of 80 mmHg, which corresponds to a normal physiologic pressure drop.

The computed flow features are compared to previous experimental data. Of particular interest is the experimental study of the SJM hinge flow fields under

aortic flow conditions conducted by Simon *et al.* using Laser Doppler Velocimetry measurements.<sup>30</sup> In this experimental study, two-dimensional phase-averaged velocity measurements were reported at selected locations along selected planes within the hinge recess. The numerical results were also compared to the flow structures qualitatively assessed using Hydrogen bubble flow visualization techniques (courtesy of Medtronic Inc). Similarly to the present numerical results, these experiments showed the existence during systole of a strong forward flow in the lateral corner of the hinge. Moreover, the simulations showed a forward flow jet of lesser magnitude and a recirculation region in the adjacent corner at different levels within the recess (Fig. 8). This recirculation region, leading to the formation of a clockwise helical flow pattern, was also observed experimentally throughout the adjacent corner<sup>30</sup> and in the *in vitro* flow visualization experiments (courtesy of Medtronic Inc). The experiments by Simon *et al.*,<sup>30</sup> along with previous experimental work,<sup>20,28</sup> report the presence of a reversal flow of low

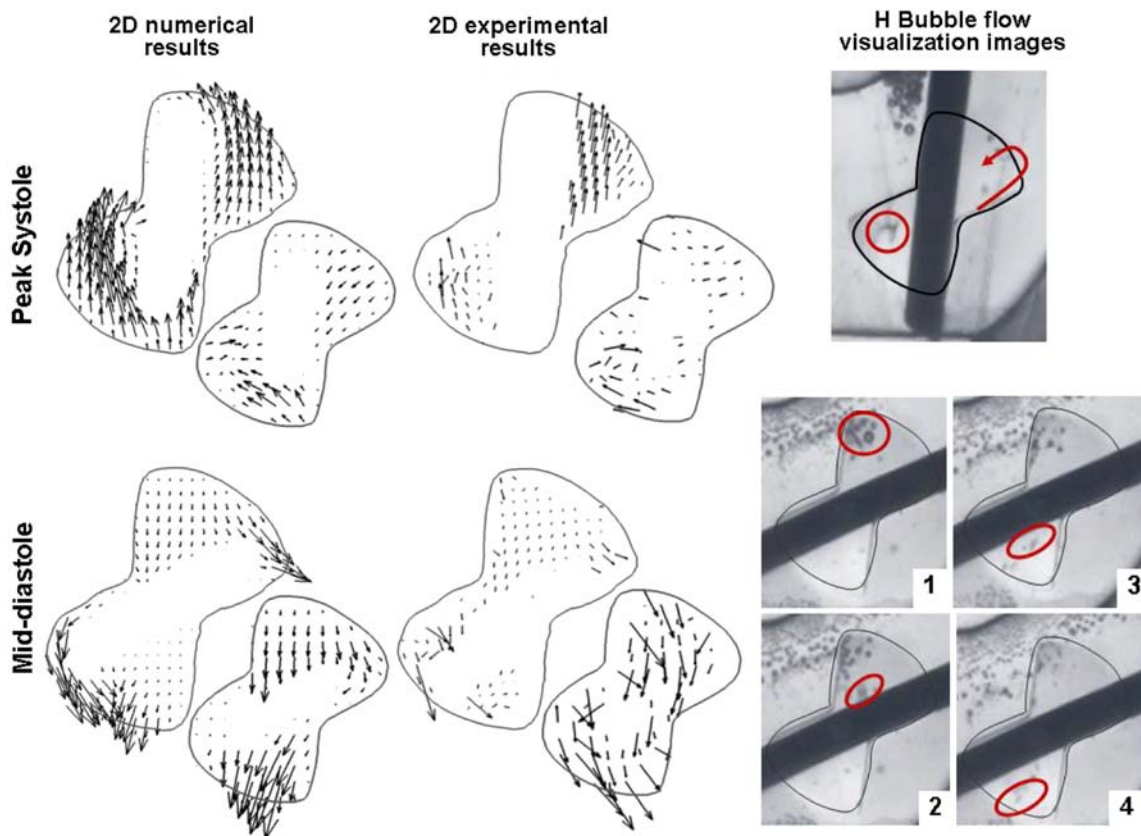


**FIGURE 8.** Comparison of the simulated and experimentally measured hinge flow structures. Two-dimensional in-plane velocity vectors are shown at the flat level of the hinge and at  $390\ \mu\text{m}$  below the flat level at peak systole and mid-diastole. The middle column shows the experimental data<sup>30</sup> and the left-most column the numerical data obtained in the present study. The right-most column shows images of the flow visualization experiments of the hinge flow fields (courtesy of Medtronic Inc). The top image shows an instantaneous image of the flow during the fully open leaflet phase, while the bottom shows a series of consecutive images acquired during diastole. The main flow features are highlighted in red.

magnitude between the leaflet ear tip and the bottom of the hinge recess that persists throughout systole even at its peak. This reverse flow region was for the first time captured using numerical simulations by Shu *et al.*<sup>29</sup> and is once again observed in the present study. This observation thus reinforces the good semi-quantitative agreement between the numerical and experimental modalities and underlines the capabilities of the current numerical solver in modeling the intricacy of the hinge flow fields.

From a quantitative viewpoint, the maximum velocity magnitude reported within the hinge recess during the forward flow phase is 1.75 m/s in the experiments<sup>30</sup> and 1.54 m/s in the present simulations. This, along with the flow structure analysis, indicates that the velocity magnitude and the general flow distribution during the forward flow phase inside the hinge recess are similar to those obtained experimentally.

At mid-diastole, good qualitative agreement is also noted between the measured and simulated flow patterns. Both experimental and simulation results revealed two main leakage flow patterns on either side of the leaflet ear and oriented toward the lateral side of the hinge. A third leakage flow pattern is seen at the flat level in the numerical results, but not in the experimental study. This could be attributed to the limited spatial resolution in the experimental measurements. It is likely that the leakage jet was not captured *in vitro*, as suggested by the small number of data points present within the ventricular corner at the flat level. Nonetheless, at deeper levels within the hinge recess (Fig. 8), the direction of the velocity vectors, and the flow visualization images, suggests the presence of this ventricular leakage jet *in vitro* (Fig. 8). Differences in velocity magnitude exist between the experimental and numerical results at mid-diastole. While the experimental study reported a maximum velocity magnitude of 2.27 m/s during the leakage phase,<sup>30</sup> the simulations show a maximum velocity field nearly twice as high with a peak of 4.75 m/s. Such a discrepancy might be attributed to the poor spatial resolution of the experiments where high velocity points might have been missed by the coarse measurement grid. However, difference in hinge gap width between the numerical and experimental models might be the predominant cause, as small changes in the gap clearance would have a strong effect on the flow magnitude. In addition, the leaflet motion in the numerical model is limited to rotation, while, in the experimental study, the leaflets are free to not only rotate but also to translate up and down along the leaflet axis. This extra degree of freedom, along with variations in manufacturing tolerances, explains the possible differences in gap clearance and thus on flow magnitude. In addition,

the limitations imposed by the numerical boundary conditions might also lead to the observed difference in flow magnitude. A full two-way coupling between the large-scale and hinge solvers is expected to yield a closer comparison between the experimental and the numerical data. Such a true multi-scale implementation, however, is beyond the scope of the present study.

The motivation behind this work is to gain a good understanding of the flow phenomena occurring inside the hinge recess to eventually relate flow structures, geometrical design, and thromboembolic potential. Assessing this potential requires (1) characterizing region of low or recirculating flow that may favor thrombus formation and (2) identifying regions of high shear stresses with elevated blood cell trauma potential. During the forward flow phase, the central region of the hinge, underneath of the leaflet ear, and the near-wall region of the adjacent hinge corner both appeared as potential zones of thrombus formation as slow flow reversal and recirculation may enhance cell-to-cell contact and favor platelet aggregation. During diastole on the other hand, the strong leakage flow pattern through the hinge and peripheral gaps prevents flow stasis. However, these fast flowing jets yield elevated viscous shear stresses, with a peak value up to 6115 dyn/cm<sup>2</sup>. The present study clearly shows that, during the leakage flow phase, regions of elevated stresses include the gap formed by the closed leaflet and the valve housing, the tip of the leaflet ear, and the wall of the ventricular side of the hinge. During the forward flow phase, on the other hand, the highest stress levels are seen immediately upstream of the hinge, along the surface of the leaflet and near the flat level. These regions, associated with elevated shear stress levels, may therefore have a great potential for inducing blood cell trauma. This suggests that the designs of the leaflet ear, the upstream section of the leaflet edge, and the hinge recess wall curvature could play an important role in the thromboembolic risk associated with the valve. It is during diastole that the largest shear stress levels were noted, suggesting that diastole might be more detrimental to blood elements than the forward flow phase. This is in agreement with previous studies.<sup>5,6,8,19,24,25,32</sup> Nonetheless, it should be pointed out that the current simulations clearly show that the shear stress levels are also elevated during systole, suggesting in particular that peak systole may be detrimental to blood elements flowing in the near hinge region. This evidence further justifies the need to simulate the hinge flow fields throughout the cardiac cycle and develop hinge recess whose design aims at minimizing flow features unfavorable to blood elements throughout the cardiac cycle.

Two major advantages of using numerical simulation as a tool for thromboembolic potential characterization

are: the ability to characterize the actual physical viscous stresses experienced by the blood cells rather than a simple surrogate such as the Reynolds shear stress commonly measured in experimental studies<sup>10</sup>; and the capability to refine the analysis to a level of spatial and temporal details not achievable experimentally. Detailed shear stress maps are critical to better locate regions potentially detrimental to blood elements. These high-resolution maps combined with a Lagrangian analysis could be used to gain a better insight of the environment experienced by blood cells by considering not only shear stress magnitude but also exposure time.

In a recently published work, Govindarajan *et al.* modeled the trajectories of platelets in the hinge region of a BMHV and attempted to estimate the potential of thrombus formation and platelet activation associated with the hinge recess.<sup>13</sup> The authors focused their analysis specifically on the valve closing phase and used a two-dimensional representation of the hinge recess. However, as emphasized by the present study, the hinge fluid dynamics is highly time-dependent and three-dimensional. Moreover, elevated shear stress levels and regions of recirculation flow, known to favor platelet activation and aggregation, are present not only during the leakage flow phase but also during the forward flow phase. The relevance of two-dimensional flow analysis to assess the blood damage potential associated by the hinge recess is thus undermined by these limitations. Lagrangian analysis of three-dimensional pulsatile hinge flow fields is expected to yield a more realistic assessment of the hinge thromboembolic potential. We are currently implementing a particle tracking algorithm to perform such an analysis on the simulated three-dimensional hinge flow fields.

### LIMITATIONS

In the present study, the selected boundary conditions ensure that the physiologic environment of the hinge is reproduced as closely as possible. However, one instance in time that the current modeling approach does not allow to capture is the instant of valve closure. This instant is modeled by prescribing the leaflet kinematics from the large-scale simulations, while pressure and flow smoothly transition toward their diastolic value. In reality, experimental studies have shown that the abrupt closure of the leaflet against the valve housing gives rise to a sudden increase in velocity magnitude and cross-valvular pressure gradient. Numerical modeling of this sudden pressure build-up would require a full two-way coupling between the large-scale and the hinge solvers to synchronize leaflet kinematics and the local hemodynamics and would

exceed currently-available computational resources. Nonetheless, the authors acknowledge that the sudden increase in cross-valvular pressure gradient at valve closure is associated with elevated shear stresses that are detrimental to blood elements.<sup>14,19,23</sup> Smoothing the valve closure flow dynamics is thus most likely leading to an underestimation of the shear stresses experienced by the blood elements.

Moreover, the blood is modeled as an incompressible single-phase Newtonian fluid. Assuming Newtonian properties and neglecting the multi-phase characteristic of the blood allows for a comparison of the numerical results with experimental findings.<sup>5,7,8,22,27,30</sup> In reality blood is a particulate fluid that exhibits non-Newtonian properties at low shear rates (shear rates less than  $100 \text{ s}^{-1}$ ). Considering a multi-phase fluid with non-Newtonian properties would yield a more realistic representation of the flow in the hinge region. Modeling the motion of single blood cells would enable estimating the actual amount of blood elements crossing through the hinge region. This could be used to estimate the survivability of red blood cells, platelets and leukocytes to the detrimental hinge flow conditions and provide a mean to quantify the blood damage specifically generated by the hinge recess alone.

### CONCLUSIONS

The present study highlights the capabilities of our numerical solver in computing the three-dimensional hinge flow fields with fine temporal and spatial resolutions. The results highlight the three-dimensionality and unsteadiness of the hinge flow fields, and their potential role in inducing blood trauma and thrombus formation. Regions of low and recirculating flow, thereby with important risk for platelet aggregation and thrombosis, were identified during systole. Regions associated with shear stress levels above the platelet activation threshold were found during systole, but it is during the leakage phase that the flow conditions are expected to be the most detrimental to the blood elements as the shear stresses computed were the highest. The results suggest that the designs of the leaflet ear, the upstream section of the leaflet edge, and the hinge recess wall curvature might play a role in the thromboembolic complications of the valve. Future work, including Lagrangian analysis of the computed flow fields, should provide a better understanding of the environment experienced by blood elements crossing the hinge and help pinpoint regions particularly unfavorable to blood elements.

## ACKNOWLEDGMENTS

This work was partially supported by a grant from the National Heart, Lung and Blood Institute (R01-HL-070262), a donation from Tom and Shirley Gurley, and the Minnesota Supercomputing Institute.

## OPEN ACCESS

This article is distributed under the terms of the Creative Commons Attribution Noncommercial License which permits any noncommercial use, distribution, and reproduction in any medium, provided the original author(s) and source are credited.

## REFERENCES

- <sup>1</sup>Balay, S., K. Buschelman, V. Eijkhout, W. D. Gropp, D. Kaushik, M. G. Knepley, L. C. McInnes, B. F. Smith, and H. Zhang. *Petsc Users Manual*. Argonne National Laboratory, 2004.
- <sup>2</sup>Balay, S., K. Buschelman, W. D. Gropp, D. Kaushik, M. G. Knepley, L. C. McInnes, B. F. Smith, and H. Zhang. *Petsc Web Page*. <http://www.Mcs.Anl.Gov/petsc>, 2001.
- <sup>3</sup>Borazjani, I., L. Ge, and F. Sotiropoulos. Curvilinear immersed boundary method for simulating fluid structure interaction with complex 3d rigid bodies. *J. Comput. Phys.* 227:7587–7620, 2008.
- <sup>4</sup>Dasi, L. P., L. Ge, H. A. Simon, F. Sotiropoulos, and A. P. Yoganathan. Vorticity dynamics of a bileaflet mechanical heart valve in an axisymmetric aorta. *Phys. Fluids* 19:067105(1)–067105(17), 2007.
- <sup>5</sup>Ellis, J., T. M. Healy, A. A. Fontaine, R. Saxena, and A. P. Yoganathan. Velocity measurements and flow patterns within the hinge region of a medtronic parallel bileaflet mechanical heart valve with clear housing. *J. Heart Valve Dis.* 5:591–599, 1996.
- <sup>6</sup>Ellis, J. T., T. M. Healy, A. A. Fontaine, M. W. Weston, C. A. Jarrett, R. Saxena, and A. P. Yoganathan. An in vitro investigation of the retrograde flow fields of two bileaflet mechanical heart valves. *J. Heart Valve Dis.* 5:600–606, 1996.
- <sup>7</sup>Ellis, J. T., B. R. Travis, and A. P. Yoganathan. An in vitro study of the hinge and near-field forward flow dynamics of the St. Jude medical® regent™ bileaflet mechanical heart valve. *Ann. Biomed. Eng.* 28:524–532, 2000.
- <sup>8</sup>Ellis, J., and A. P. Yoganathan. A comparison of the hinge and near-hinge flow fields of the St. Jude medical hemodynamic plus and regent bileaflet mechanical heart valves. *J. Thorac. Cardiovasc. Surg.* 119:83–93, 2000.
- <sup>9</sup>Gao, Z. B., N. Hosein, F. F. Dai, and N. H. C. Hwang. Pressure and flow fields in the hinge region of bileaflet mechanical heart valves. *J. Heart Valve Dis.* 8:197–205, 1999.
- <sup>10</sup>Ge, L., L. P. Dasi, F. Sotiropoulos, and A. P. Yoganathan. Characterization of hemodynamic forces induced by mechanical heart valves: Reynolds vs. Viscous stresses. *Ann. Biomed. Eng.* 36:276–297, 2008.
- <sup>11</sup>Ge, L., and F. Sotiropoulos. A numerical method for solving the 3d unsteady incompressible Navier–Stokes equations in curvilinear domains with complex immersed boundaries. *J. Comput. Phys.* 225:1782–1809, 2007.
- <sup>12</sup>Gilmanov, A., and F. Sotiropoulos. A hybrid cartesian/immersed boundary method for simulating flows with 3d, geometrically complex, moving bodies. *J. Comput. Phys.* 207:457–492, 2005.
- <sup>13</sup>Govindarajan, V., H. S. Udaykumar, and K. B. Chandran. Two-dimensional simulation of flow and platelet dynamics in the hinge region of a mechanical heart valve. *J. Biomech. Eng.* 131:031002, 2009.
- <sup>14</sup>Graf, T., H. Fisher, H. Reul, and G. Rau. Cavitation potential of mechanical heart valve prostheses. *Int. J. Artif. Organs* 14:169–174, 1991.
- <sup>15</sup>Gross, J. M., M. C. S. Shu, F. F. Dai, J. Ellis, and A. P. Yoganathan. A microstructural flow analysis within a bileaflet mechanical heart valve hinge. *J. Heart Valve Dis.* 5:581–590, 1996.
- <sup>16</sup>Higdon, A., E. H. Ohlsen, W. Stiles, J. Weese, and W. Riley. *Mechanics of Material*. New York: Wiley, 1985.
- <sup>17</sup>Hung, T. C., R. M. Hochmuth, J. H. Joist, and S. P. Suter. Shear-induced aggregation and lysis of platelets. *Trans. Am. Soc. Artif. Intern. Organs* 22:285–291, 1976.
- <sup>18</sup>Kelly, S. G. D., P. R. Verdonck, J. A. M. Vierendeels, K. Rienslagh, E. Dick, and G. Van Nooten. A three-dimensional analysis of flow in the pivot regions of an ats bileaflet valve. *Int. J. Artif. Organs* 22:754–763, 1999.
- <sup>19</sup>Lamson, T. C., G. Rosenberg, D. B. Geselowitz, S. Deutsch, D. R. Stinebring, J. A. Frangos, and J. M. Tarbell. Relative blood damage in the three phases of a prosthetic heart valve flow cycle. *ASAIO J.* 39:M626–M633, 1993.
- <sup>20</sup>Leo, H.-L. An In Vitro Investigation of the Flow Fields Through Bileaflet and Polymeric Prosthetic Heart Valves. Ph.D. thesis, Biomedical Engineering Department, Georgia Institute of Technology, 2005.
- <sup>21</sup>Leo, H.-L., Z. He, J. T. Ellis, and A. P. Yoganathan. Microflow fields in the hinge region of the carbomedics bileaflet mechanical heart valve design. *J. Thorac. Cardiovasc. Surg.* 124:561–574, 2002.
- <sup>22</sup>Leo, H.-L., H. A. Simon, L. P. Dasi, and A. P. Yoganathan. Effect of hinge gap width on the microflow structures in 27-mm bileaflet mechanical heart valves. *J. Heart Valve Dis.* 15:800–808, 2006.
- <sup>23</sup>Liu, Y., S. Aluri, W. Richenbacher, and K. B. Chandran. Red cell damage in flexible leaflet heart valves. In: Annual Fall Meeting of the Biomedical Engineering Soc, Atlanta, GA, 1999.
- <sup>24</sup>Maymir, J.-C., S. Deutsch, R. S. Meyer, D. B. Geselowitz, and J. M. Tarbell. Effects of tilting disk heart valve gap width on regurgitant flow through an artificial heart valve. *Artif. Organs* 21:1014–1025, 1997.
- <sup>25</sup>Meyer, R. S., S. Deutsch, J.-C. Maymir, D. B. Geselowitz, and J. M. Tarbell. Three-component laser doppler velocimetry measurements in the regurgitant flow region of a bjork-shiley monostrut mitral valve. *Ann. Biomed. Eng.* 25:1081–1091, 1997.
- <sup>26</sup>Ramstack, J. M., L. Zuckerman, and L. F. Mockros. Shear-induced activation of platelet. *J. Biomech.* 12:113–125, 1979.
- <sup>27</sup>Saxena, R., J. Lemmon, J. Ellis, and A. P. Yoganathan. An in vitro assessment by means of laser doppler velocimetry of the medtronic advantage bileaflet mechanical heart valve hinge flow. *J. Thorac. Cardiovasc. Surg.* 126:90–98, 2003.
- <sup>28</sup>Shu, M. C. S., J. M. Gross, K. K. O'Rourke, and A. P. Yoganathan. An integrated macro/micro approach to evaluating pivot flow within the medtronic advantage (tm)

- bileaflet mechanical heart valve. *J. Heart Valve Dis.* 12:503–512, 2003.
- <sup>29</sup>Shu, M. C. S., K. K. O'Rourke, C. M. Coppin, and J. D. Lemmon. Flow characterization of the advantage<sup>®</sup> and St. Jude medical<sup>®</sup> bileaflet mechanical heart valves. *J. Heart Valve Dis.* 13:814–822, 2004.
- <sup>30</sup>Simon, H. A., H.-L. Leo, J. Carberry, and A. P. Yoganathan. Comparison of the hinge flow fields of two bileaflet mechanical heart valves under aortic and mitral conditions. *Ann. Biomed. Eng.* 32:1607–1617, 2004.
- <sup>31</sup>Sotiropoulos, F., and I. Borazjani. A review of the state-of-the-art numerical methods for simulating flow through mechanical heart valves. *Med. Biol. Eng. Comput.* 47:245–256, 2009.
- <sup>32</sup>Steeegers, A., R. Paul, H. Reul, and G. Rau. Leakage flow at mechanical heart valve prostheses: improved washout or increased blood damage? *J. Heart Valve Dis.* 8:312–323, 1999.
- <sup>33</sup>Wang, J. W., H. Yao, C. J. Lim, Y. Zhao, T. J. H. Yeo, and N. H. C. Hwang. Computational fluid dynamics study of a protruded-hinge bileaflet mechanical heart valve. *J. Heart Valve Dis.* 10:254–263, 2001.
- <sup>34</sup>Wurzinger, L. J., R. Opitz, and H. Eckstein. Mechanical blood trauma: an overview. *Angeiologie* 38:81–97, 1986.
- <sup>35</sup>Wurzinger, L. J., R. Opitz, M. Wolf, and H. Schmid-Schönbein. Shear induced platelet activation—a critical reappraisal. *Biorheology* 22:399–413, 1985.